1999 Turbomachinery Committee Best Paper Award

Development of Advanced Compressor Airfoils for Heavy-Duty Gas Turbines—Part I: Design and Optimization

Ulf Köller
Reinhard Mönig

Siemens AG,
Power Generation (KWU)
D-45466 Mülheim a. d. Ruhr, Germany

Bernhard Küsters
Heinz-Adolf Schreiber

German Aerospace Center,
Institute of Propulsion Technology,
D-51170 Köln, Germany

A new family of subsonic compressor airfoils, which are characterized by low losses and wide operating ranges, has been designed for use in heavy-duty gas turbines. In particular the influence of the higher airfoil Reynolds numbers compared to aeroengine compressors and the impact of these differences on the location of transition are taken into account. The design process itself is carried out by the combination of a geometric code for the airfoil description, with a blade-to-blade solver and a numerical optimization algorithm. The optimization process includes the design-point losses for a specified Q3D flow problem and the off-design performance for the entire operating range. The family covers a wide range of inlet flow angle, Mach number, flow turning, blade thickness, solidity and AVDR in order to consider the entire range of flow conditions that occur in practical compressor design. The superior performance of the new airfoil family is demonstrated by a comparison with conventional controlled diffusion airfoils (CDA). The advantage in performance has been confirmed by detailed experimental investigations, which will be presented in Part II of the paper. This leads to the conclusion that CDA airfoils that have been primarily developed for aeroengine applications are not the optimum solution, if directly transferred to heavy-duty gas turbines. A significant improvement in compressor efficiency is possible, if the new profiles are used instead of conventional airfoils. [S0889-504X(00)02102-4]

Introduction

Modern heavy-duty gas turbine compressors used in combined cycle operation have to deal with a number of requirements. Due to economical and ecological demands, high efficiency as well as higher power output, based on both growing mass flows and increasing specific work, are desired. Gas turbines have to operate with sufficient surge margin in different climate conditions, at rotating speed variations due to frequency deviation in the power supply system, and at part-load conditions. These requirements can only be satisfied, if within the design process both the static and dynamic strength demands and the aerodynamic performance of the compressor blades are taken into account. The stacking of the profiles in the radial direction, as well as the profiles themselves, play an important role for the efficiency and the operational safety of the whole compressor.

Due to the high mass flow, the front compressor stages have to deal with transonic and supercritical velocity distributions, while in the middle and the rear stages subsonic flow is predominant. In this subsonic region it is very efficient to use profile families for blading in order to achieve a fast and reliable compressor design. The quality of an airfoil is mainly determined by the total pressure losses and the attainable operating range.

In the past, different airfoil families have been developed for use in subsonic compressor design. Based on extensive experimental studies, the NACA-65 airfoils [1] were implemented in many aeroengine and heavy-duty gas turbines. From the end of the seventies controlled-diffusion airfoils (CDA) made their way into modern compressor design, which were based on both experimental and numerical research work [2]. For the design process itself, two different computer-aided methods are commonly in use: the direct and the inverse approach. In the direct method, the flow field is completely described by the specified cascade geometry and the flow conditions up- and downstream of the cascade. The inverse approach is based on the velocity distribution on the profile surfaces. Together with a given solidity and the inlet/exit flow conditions, the associated airfoil geometry can be defined [3,4]. However, this inverse design method requires multiple variations of the velocity distribution until an acceptable profile geometry is obtained. The first supercritical airfoil, which was designed by the inverse approach and validated by experimental results, was presented by Stephens [5]. In the following years many authors showed the superiority of the new design, both for supercritical and subsonic airfoils [6,7].

In the same way as gas turbines have to work at part-load, the compressor airfoils have to operate at off-design conditions, which means different inlet flow angles, Mach numbers, and axial velocity density ratios. By using an inverse approach, it is not possible to consider the cascade's performance at part-load conditions. Only the employment of a direct flow solver can provide information on the airfoil's off-design behavior.

A second reason for using the direct method is to enable the coupling of the flow solver with an optimization algorithm and a geometric code for the airfoil description in order to achieve an automated design tool. The variables needed as input to the geometric code can be used as independent variables for the optimization process. With the use of an automated approach, a large number of airfoil designs can be carried out, which is required to establish a new airfoil family. This idea of automated design has already been presented by Sanger [8] and used for optimizing the design of a controlled-diffusion stator blade row. With the increasing calculation capacity of modern computers, the employ-

Contributed by the International Gas Turbine Institute and presented at the 44th International Gas Turbine and Aeroengine Congress and Exhibition, Indianapolis, Indiana, June 7–10, 1999. Manuscript received by the International Gas Turbine Institute February 1999. Paper No. 99-GT-95. Review Chair: D. C. Wisler.

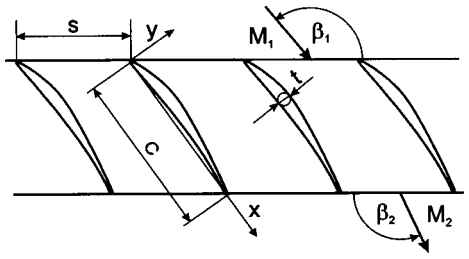

Fig. 1 Aerodynamic and geometric cascade parameters

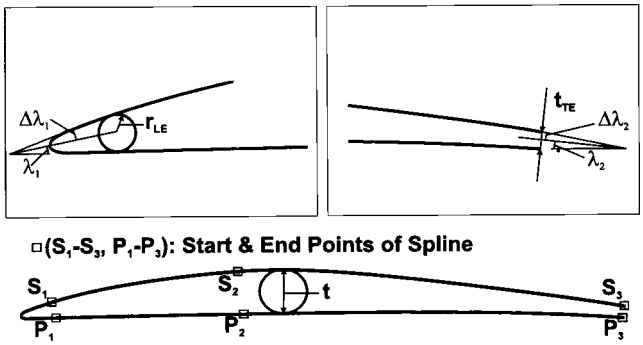

Fig. 2 Design parameters for airfoil generation

ment of such coupled, automated design tools is still rising, Sanz [9] used an inverse hodograph method in conjunction with an optimization algorithm, Goel et al. [10] extended the use of this automated design to turbine airfoils and Pierret et al. [11] coupled a Navier–Stokes solver with an artificial neural network. Even algorithms based on genetic ideas made their way into airfoil design [12] and optimization is now used for solving different problems in turbomachinery [13]. But in all these airfoil design procedures, the off-design behavior is excluded.

Today in most heavy-duty gas turbines NACA-65 or CDA profiles are in use for designing the subsonic compressor stages. While the NACA-65 profiles were initially developed as airfoil profiles, the controlled-diffusion airfoils were originally designed for use in supercritical cascades. Hence, both families were not initially designed for use in subsonic heavy-duty gas turbine compressor stages. So the question must be raised: Do these airfoils represent an optimal solution to meet the requirements of such large compressors, where the profile loss and the airfoil's operating range are of utmost importance?

This paper deals with the development and experimental validation of a new compressor airfoil family under consideration of the special flow boundary conditions in a heavy-duty gas turbine compressor (Fig. 1). A direct approach is used because the design and the off-design behavior of the cascades need to be taken into account. As the profile geometry can be described by a number of geometric parameters, the search for an optimal airfoil geometry can be transferred to an optimum search in a multidimensional space and can be solved with a modern numerical optimization algorithm. Based on a variety of optimized profiles, a new airfoil family was created that covers the wide range of mechanical and aerodynamic properties of the multistage axial compressor. Detailed experimental investigations, carried out in the DLR transonic cascade wind tunnel, confirmed the superiority of the optimized profiles. The corresponding results are presented in Part II of this paper [14].

Analysis Methods

The airfoil design process used for the development of the new profile family is carried out automatically by the combination of a geometric code for the airfoil description with a blade-to-blade solver and a numerical optimization algorithm.

Profile Model. The geometry model implemented allows a direct description of the airfoil surfaces. As the suction side diffusion is mainly responsible for the profile losses at design conditions, the profile generation starts with the suction side construction and then attaches the pressure side.

Figure 2 gives an example of the airfoil geometry. For the construction of each surface two third-order spline functions are used. The leading edge geometry is described by an elliptical function, the trailing edge by a circular arc. In general a spline function definition requires the start and end point coordinates as well as the referring slopes. The leading edge enlargement shows the parameters used in this geometry model to define the coordinates and the slope at the suction side starting point S_1: the leading edge radius $r_{L\epsilon}$, the inlet metal angle λ_1, and the wedge angle $\Delta\lambda_1$. Together with the x/y coordinates at location S_2 (the connection between the two suction side splines) and the corresponding data for the trailing edge, the two spline functions (from S_1 to S_2 and from S_2 to S_3) can be calculated. The pressure side is attached with the requirement that the maximum airfoil thickness matches the prescribed value of t. In a further step the circular leading edge is modified to an elliptical one.

The effectiveness and flexibility of this model is demonstrated in Fig. 3 by the reproduction of three given airfoil geometries. In the top diagram a controlled-diffusion airfoil of the V84.3A-Siemens gas turbine [15] is shown. The next airfoil was designed using the inverse approach for application in the first rotor hub section of an industrial compressor [16] and the third diagram shows an inverse designed high turning stator cross section [6]. All three reproductions are almost congruent with the original geometries. This underlines the flexibility of the geometry program to construct arbitrary profiles, which is necessary to allow a successful optimization process.

Blade-to-Blade Calculation Method. All calculations presented in Part I have been carried out with the inviscid/viscous flow solver MISES developed at MIT by Giles [17] and Drela [18]. A two-dimensional, steady-state and inviscid calculation of the flow field is coupled with an integral, compressible boundary layer calculation. The influence of the stream tube height is taken into account and for local supersonic regions the ''artificial viscosity'' formulation is implemented. The flow is discretized by a finite-volume approach, where two of the four element edges are identical to the streamlines. The corresponding computational grid topology and an enlargement of the leading edge region are shown in Fig. 4.

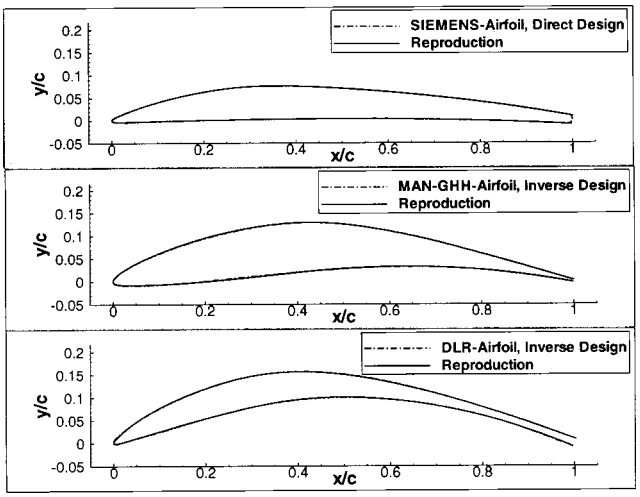

Fig. 3 Reproduction of three compressor profiles

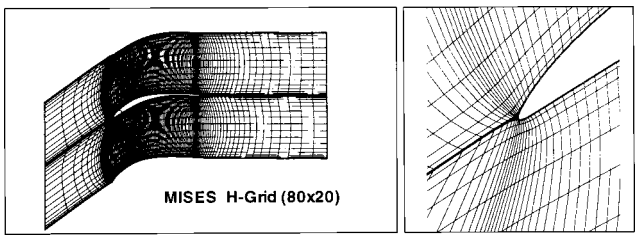

Fig. 4 Computational grid for subsonic compressor airfoil

Based on the inviscid flow results and the airfoil surface geometry, an integral calculation of the two-dimensional, compressible laminar and turbulent boundary layer equations is carried out during each iteration step of the flow solver. The laminar–turbulent transition can occur in three different modes depending on the free-stream turbulence level, the Reynolds number, and the pressure distribution: free, bypass, and transition in combination with a separation bubble [18,19]. Inviscid and viscous code elements are coupled by the displacement thickness. Contrary to most inviscid/viscous codes, MISES solves the boundary layer equations together with the flow field as a coupled system. After each iteration step, the computational grid node coordinates are adapted to the local flow conditions, so that in a converged solution the grid lines in the main flow direction coalesce with the stream lines. The exit flow angle and the total pressure loss are calculated by conservation of mass, momentum, and energy from the cascade exit to a specified mixing plane downstream.

For a first validation, experimental data and MISES calculations of the two inverse designed airfoils shown in Fig. 3 have been compared. Fig. 5 and Table 1 show the results for the MANGHH-Airfoil [16] at design point conditions with more than 38 deg of flow turning. The calculated Mach number distribution is in excellent agreement with the experimental data for both suction and pressure side. Static pressure rise, exit Mach number, and total pressure loss show a very good agreement and exit flow angle difference seems to be near the measurement accuracy. The MISES validation prior to the design of the new airfoil familiy was extended to the comparison of the complete operating range for both inverse designed airfoils. MISES showed satisfying agreement to the experimental data in all regarded conditions, so these first results confirmed the choice of MISES as the preferred flow solver for the intended airfoil design.

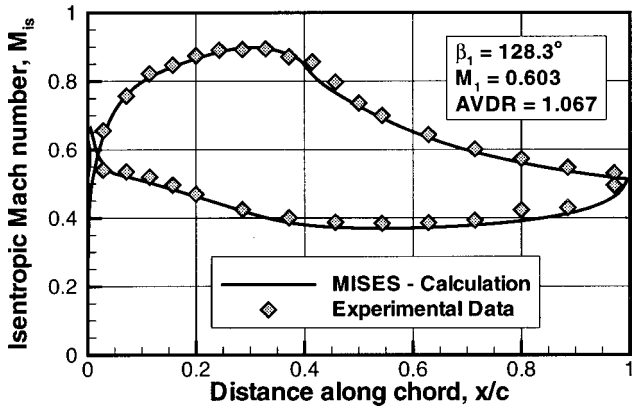

Fig. 5 MISES and experimental Mach number distribution

Table 1 Numerical and experimental exit data

	β_2	M_2	ω	p_2/p_1
MISES	89.7°	0.466	1.51%	1.098
Experiment	90.4°	0.466	1.45%	1.098

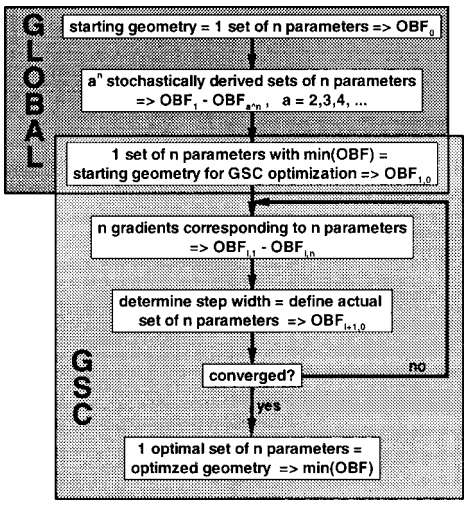

Fig. 6 Flowchart of optimization algorithm

Optimization Algorithm. The goal of each optimization process is the minimization or maximization of an objective function. Use of the geometric parameters ($\lambda_1, \Delta\lambda_1, r_{LE}, \lambda_2, \Delta\lambda_2, t_{TE}, \ldots$) shown in Fig. 2 as optimization parameters for this process leads to an optimal airfoil design with respect to the given objective function. For each parameter lower and upper bounds have to be defined in order to avoid physically meaningless solutions. These definition ranges are also used for the normalization of each parameter. This allows comparison of parameter gradients based on different dimensions. The choice of which optimization algorithm should be adopted to solve a given problem depends strongly on the mathematical properties of the objective function. The higher the objective function's order of steadiness is, the more sophisticated the chosen optimization algorithm can be. But the question of whether the optimum reached is a global or local one cannot be answered.

For the optimization presented in this paper, a combination of two algorithms has been adopted: a normal-distributed random search code (GLOBAL) together with the deterministic Gauss–Seidel-Coordinate (GSC) strategy, which basically is a gradient method. A fundamental description of both is presented by Schwarz and Spiegel [13] and the corresponding flowchart is shown in Fig. 6. Each objective function call means blade-to-blade calculations for the stagger angle determination, the design and the off-design behavior for a given geometry (= set of n parameters) and is symbolized by ''⇒'' in the flowchart. Hence, for a certain airfoil the requested flow turning is achieved by the determination of the required stagger angle through preliminary blade-to-blade calculations in each objective function call.

At the beginning the user has to define one set of n parameters, which represent the initial (starting) geometry and the basis ''a'' for the random search code. Within the given definition ranges, a normal distribution of each parameter is generated with each starting parameter as an expected value and a preliminary user-specified standard deviation. For each of the so-derived a^n sets of parameters the objective function values are calculated. As the chosen objective function includes the calculation of the cascade's design and off-design behavior, the random search basis ''a'' was set to $a=2$. With a number of parameters ''n'' used in the optimization process between $n=6$ and $n=10$. a^n was in the range of 64 to 1024. That set of parameters, identified by the minimal objective function value, serves as input/starting geometry for the GSC strategy. Each GSC iteration cycle consists of three steps:

- search for the optimization direction in the n-dimensional space,

- determine the step width for the found optimization direction (leads to a new set of *n* parameters),
- check all defined convergence criteria.

The optimal set of *n* parameters defines the geometry, which with respect to the objective function, repesents an optimal solution for the given problem. The higher the number *a* and the standard deviation in the random algorithm are, the more global the search is.

The combination of the three presented codes, the geometric profile model, the blade-to-blade flow solver, and the optimization algorithm together with a given objective function, enables the user to automatically design airfoils for a given vector diagram.

Airfoil Design

The prescribed tool for automated airfoil design has been used for a wide range of application. Based on a large number of optimizations, a new airfoil family has been developed.

Range of Application. Because an airfoil family used for the whole subsonic compressor has to cover flow turning problems for both the mid and the rear part of the compressor, for both the hub and the tip endwall blading, for both stators and rotors and for different reaction numbers, each considered variation parameter has to cover a wide range. In Table 2 the minimum and maximum values for each design parameter are given. One discrete value for each design parameter (β_1, $\Delta\beta$, M_1, t/c, s/c, and *AVDR*) is established in order to define one flow problem, which is to be solved by the automated design tool. Within these ranges only design relevant combinations of parameters have been adopted as a basis for the new airfoil family.

Objective Function. Apart from the flow solver the quality of optimization results depend mainly on the optimization algorithm itself and on the formulation of the objective function. If this formulation mathematically represents the desired physical behavior, a good design can be expected by using an optimization process. So the validation of a chosen objective function is one key to a successful automatic airfoil design.

As mentioned above, modern heavy-duty gas turbine compressors have to operate with high efficiency at varying conditions. This primarily means that the level of the total pressure loss at the design point and the entire incidence range of the cascade is essential for the compressor performance. Figure 7 illustrates all elements used for the objective function, which takes into account the complete airfoil's operating range. The corresponding formulation of the objective function is

$$\mathrm{OBF}=C_1\cdot\frac{\omega_D}{\omega_{\mathrm{ref}}}+C_2\cdot\frac{\Delta\beta_1}{\Delta\beta_{1,\mathrm{ref}}}+C_3\cdot\frac{\left|(\Delta\beta_{St}/\Delta\beta_1)-(\Delta\beta_{St}/\Delta\beta_1)_{\mathrm{ref}}\right|}{(\Delta\beta_{St}/\Delta\beta_1)_{\mathrm{ref}}}+C_4\cdot\frac{\omega_{80}}{\omega_{80,\mathrm{ref}}}+C_5\cdot\frac{\sigma_{80}}{\sigma_{80,\mathrm{ref}}}+\Sigma PF. \quad (1)$$

The total pressure loss at design conditions is called ω_D. The limits of the attainable operating range $\Delta\beta_1$ are defined by twice the value of ω_D. The relative stall margin is given by the expression $(\Delta\beta_{St}/\Delta\beta_1)$. To aspire to a ''flat'' loss curve, the mean value of the total pressure losses for the inner 80 percent of the operating range is called ω_{80} and the corresponding standard deviation σ_{80}. The abbreviation *PF* represents the penalty function

Table 2 Range of design parameters

	β_1	$\Delta\beta$	M_1	t/c	s/c	$AVDR$
Min	130^o	4^o	0.35	0.04	0.7	0.9
Max	165^o	30^o	0.80	0.16	1.2	1.2

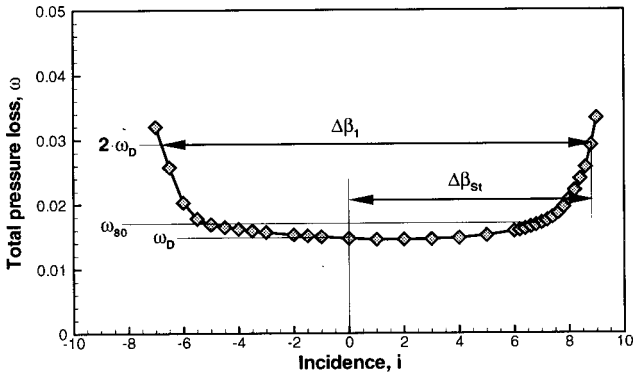

Fig. 7 Elements for objective function definition

terms, which introduce geometric restrictions for a mathematical formulation. For instance, due to static and dynamic strength requirements the cross section area of a rotor blade may not be less than a certain given value. If during the optimization process a geometry is generated that fails this criterion, a relating number *PF* will be added to the objective function value OBF. The reference values allow a normalization of the different objective function terms. The coefficients *C* are used for weighting each term against the others and must be specified by the user and validated by test runs of the design tool. The objective of the optimization process is to minimize this function.

With this type of objective function a design will be achieved, which is characterized by:

- low loss at design point condition;
- a wide operating range;
- a definite relative stall margin:
- a low and constant loss level within the inner 80 percent incidence range;
- no violation of any geometric restrictions.

This formulation represents a new approach in automated airfoil design, because the cascade's complete operating range is taken into account.

Airfoil Optimization. To give an impression of the presented tool's and objective function's efficiency, an optimization example will be presented and discussed in detail. Figures 8–10 show comparisons between the profile before and after the optimization. In the lower diagram of Fig. 8 the design point and cascade data (β_1, $\Delta\beta$, M_1, t/c, s/c, and AVDR) are noted. With a diffusion factor of $DF=0.42$, the loading of this cascade is

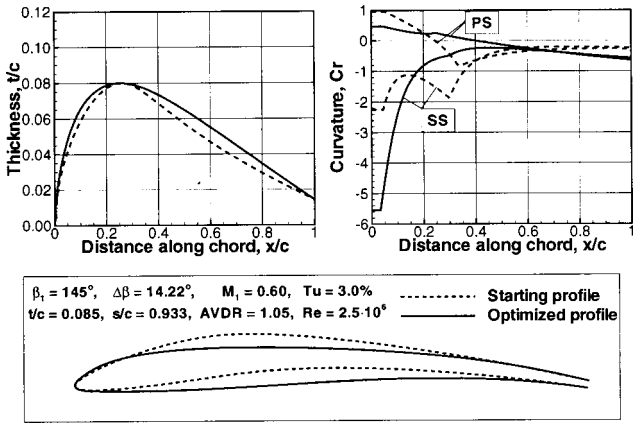

Fig. 8 Geometry of starting and optimized profiles

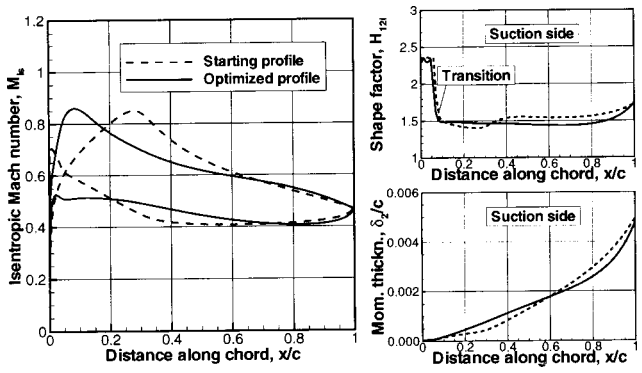

Fig. 9 Mach number distributions and boundary layer parameters for starting and optimized profiles

within an usual range for subsonic heavy-duty gas turbine compressor airfoils. The Reynolds number is set to 2.5×10^6 and the turbulence level to a value where bypass transition is predominant. That means that transition occurs at a location where the momentum thickness Reynolds number approaches a value of roughly 200.

As the upper left diagram shows, both geometries, the starting and the optimized design, have the same x/c value for the maximal thickness t/c at 25 percent. The thickness of the optimized profile in front of and behind the maximum is higher, because the starting airfoil's cross section area is too small and leads to a violation of the corresponding mechanical restriction. In the upper right diagram the curvature distributions of suction and pressure side are presented. The greatest differences appear on the front part of the suction side distribution, where the optimized airfoil has curvature values below -5. This strong curvature leads to an almost flattend midpart of the suction side, as shown in the lower diagram of Fig. 8. The front wedge angle $\Delta\lambda_1$ has been considerably increased during the optimization process, which results in a thicker leading edge geometry. At the trailing edge both surfaces of the optimized airfoil are characterized by an increase in curvature and a higher rear wedge angle $\Delta\lambda_2$.

Comparing the Mach number distributions for design conditions in Fig. 9, the most significant difference is visible in the upstream propagation of the peak suction side Mach number for the optimized airfoil. As shown in the upper diagram on the right side, the laminar–turbulent transition on the suction side is located upstream of 10 percent chord. Suction side diffusion starts shortly after the transition location, when the turbulent boundary

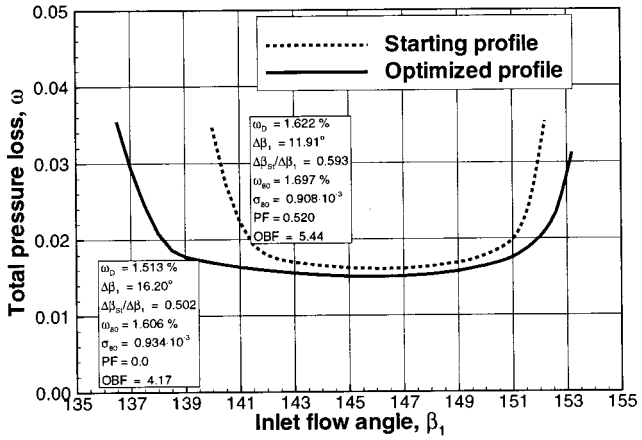

Fig. 10 Total pressure losses of starting and optimized profiles

layer is still thin. On the one hand this means that in the front accelerated part the boundary layer of the starting profile is already turbulent. On the other hand this leads to a smaller deceleration gradient for the optimized airfoil downstream of the peak Mach number. With incompressible shape factor values below 1.8, both airfoils show significant margin to suction side separation, which is assumed to occur at H_{12i} values between 2.5 and 3.0. The suction side boundary layer momentum thickness distributions are presented in the lower diagram on the right side. In conjunction with the Mach number distributions, the important role of the deceleration gradients can be clearly seen: The higher the local deceleration gradient is, the higher the local momentum thickness growth rate is. For instance, between 30 and 70 percent of chord, the diffusion on the starting geometry is significantly higher and the boundary layer momentum thickness grows with a higher gradient, as well. At the trailing edge of the starting profile the momentum thickness is slightly higher than for the optimized geometry.

The total pressure losses for both airfoils are presented in Fig. 10. In addition, the corresponding elements of the objective function are noted. With regard to the starting profile, the design losses have been reduced by more than 6 percent, the incidence range has been increased by more than 4 deg, including 1 deg larger stall margin, and the penalty function value has been reduced to zero. Correspondingly, the objective function value could be reduced from 5.44 to 4.17. The main cause of the increased operating range is the thicker leading edge geometry, which is less sensitive to any off-design inlet flow angle. The almost flattened midpart of the profile and the smaller trailing edge momentum thickness values lead to the reduced design point losses.

The considerable improvement in the design and the off-design behavior of the optimized profile proves the efficiency in airfoil design of both the optimization process and the objective function formulation. The starting profile's Mach number distribution with its acceleration until $x/c=30$ percent resembles closely a CDA-type distribution. For most of the CDA designs, apparently, it has been assumed that laminar flow is present on the suction side, at least partly up to 20–30 percent of chord. The new optimized airfoils, however, consider the effect of early transition at the high Reynolds number and turbomachinery turbulence level.

This optimization process has been carried out for approximately 400 airfoil designs in order to get enough optimal profiles as a basis for the new airfoil family. All design calculations have been carried out at a Reynolds number $\mathrm{Re}=2.5\times10^6$, which represents an average for the blading in a real large-scale heavy-duty gas turbine compressor. Because the turbulence level is about 3 percent and higher in the mid- and rear-part compressor stages [20] and as further increase in turbulence level hardly affects the MISES-calculated transition location at Reynolds numbers higher than 2×10^6 (see also last section of this paper and Fig. 15), the turbulence level was set to a value of $Tu=3$ percent.

The optimization results have been used as a data basis to develop correlations for each geometric parameter as a function of the six varied flow and cascade parameters (β_1, $\Delta\beta$, M_1, t/c, s/c, and AVDR). Using these correlations in compressor design leads to an extremely fast and efficient blading design. In contrast to conventional airfoil families where geometric input like stagger, inlet, and outlet metal angles is needed, only the six flow and cascade parameters have to be defined. As a two-dimensional duct- or throughflow compressor design calculation results in the radial distributions of the flow properties in the axial gaps, all six parameters for each cross section in the flow path are given and the corresponding airfoil geometry is directly determined by the developed correlations. In order to validate these correlations and the corresponding airfoil family, a four-step process has been adopted:

- Check airfoil geometry within given ranges of application for violation of geometric restrictions.
- Check objective function curves/planes of the new airfoil

Table 3 Design parameters of test cascades A–D

Cascade	A	B	C	D
M_1	0.715	0.607	0.556	0.438
β_1	149.4°	142.0°	147.3°	137.0°
$\Delta\beta$	10.3°	14.7°	12.8°	18.0°
t/c	5.0%	7.0%	7.4%	9.3%
s/c	0.855	0.888	0.953	0.874
$AVDR$	1.06	1.05	1.05	0.99
DF	0.393	0.393	0.407	0.422

family for unusually high values in order to determine regions where the geometric correlations do not match the support points/results from the optimization process.

- Compare geometry and objective function values of an optimized airfoil with the corresponding representative of the new family for arbitrary combinations of the six flow and cascade parameters.
- Compare representatives of the new airfoil family with conventional controlled-diffusion airfoils.

Steps one and two were performed for more than 4000 geometries. In those parts of the range of application where these checks revealed unsatisfying results, the correlations have been corrected. In the third step for about ten combinations of the six flow and cascade parameters, new optimizations have been performed and their results have been compared to the representatives of the new airfoil family. All examples showed almost no changes in airfoil geometry and the decrease in the objective function value was negligible. As a part of the validation of this new approach, four examples for the step four comparisons are presented in the following section.

Comparison to Reference CDA Cascades. For the experimental investigation of the new airfoil family [14] four cascades have been selected, which are typical representatives for rotor and stator sections in the mid and rear part of a compressor [21]. The design parameters together with the diffusion factors are presented in Table 3. For these parameters, four profiles (A–D) have been adopted from the new airfoil family, where the inlet Mach number is decreased from cascade A to D. In order to demonstrate the superior behavior of the new design, four controlled-diffusion airfoils have been selected, which satisfy the same design requirements.

A comparison of the airfoil geometries is presented in Fig. 11. As the inlet Mach number decreases, the new (test) profiles show smaller stagger angles than the controlled-diffusion airfoils. Similar to the earlier example (Fig. 8), the new airfoils show more camber in the front and less camber in the midportion, and the leading edge geometries are thicker compared to the CDA shape.

The corresponding design point Mach number distributions are shown in Fig. 12. All test profiles are characterized by a front-loaded pressure distribution, boundary layer transition shortly before the velocity maximum at about 7–10 percent chord, and smaller deceleration gradients in the midpart of the airfoils. The differences between the new and the CDA design increase from

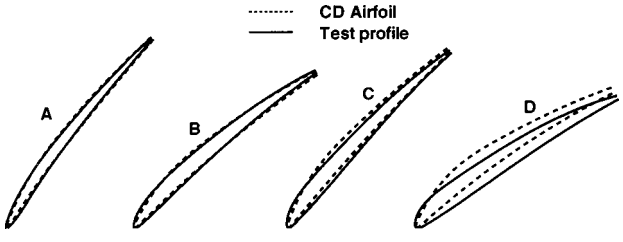

Fig. 11 Geometry of CDA and new airfoils

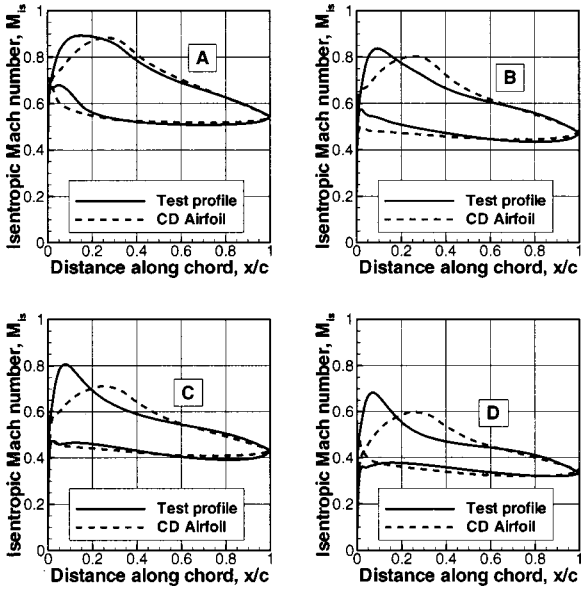

Fig. 12 Design Mach number distributions of CDA and new airfoils

cascade A to D (Fig. 11), which are characterized by decreasing inlet Mach numbers. As controlled diffusion airfoils were initially designed for use in supercritical and high subsonic applications and afterward transferred to use in mid and low subsonic stages, in particular the low subsonic airfoils show significant changes in design. In contrast, cascade A is quite similar for both designs, as a significantly increased front loading based on a thicker leading edge for the test profile would result in a local transonic flow region and lead to higher total pressure losses.

Figure 13 presents the total pressure losses for all four test profiles together with the corresponding controlled-diffusion airfoils. All representatives of the new airfoil family are characterized by increased operating ranges, including higher incidence range to stall. The highest growth can be seen for cascade B, where the stall margin rises from 5 deg for the CDA to 9 deg; all three other airfoils show an increase in stall margin of at least 1.5 deg. All four new profiles likewise show lower total pressure losses over the entire operating ranges.

In order to demonstrate the achievable benefit of this new airfoil family on the compressor efficiency and cost, additional loss curves (dash-dotted lines) are included in all four diagrams of Fig. 13. The five design parameters M_1, β_1, $\Delta\beta$, t/c, and AVDR are kept at the same values already presented in Table 3, while the pitch-to-chord ratios are increased. For the test case D the same stall margin as for the controlled diffusion airfoil has been achieved by adopting a pitch-to-chord ratio of 1.05. Even with the maximum pitch-to-chord ratio covered in the range of application, the stall margins for the increased-pitch airfoils of test cases A–C are still higher than for the CD airfoils. Hence, for the presented comparisons (A–C) a s/c value of 1.2 has been adopted. As the stall margin (compared to CDA) does not decrease, the same compressor operation range can be guaranted based on reduced numbers of blades and vanes. In all four cases a significant reduction in the total pressure losses for the entire operating ranges is visible. At design point conditions the losses are decreased by 20 percent. Based on this example a compressor efficiency rise of 1 percent and more can be expected.

In order to elucidate the reasons for the considerable increase in operating range the Mach number distributions at -5 deg and $+5$ deg incidence for cascade C are compared in Fig. 14. The corresponding incidence flow angles are marked in the total pressure loss diagram in Fig. 13. The importance of the thickened leading edge vicinity is demonstrated by the off-design behavior of test

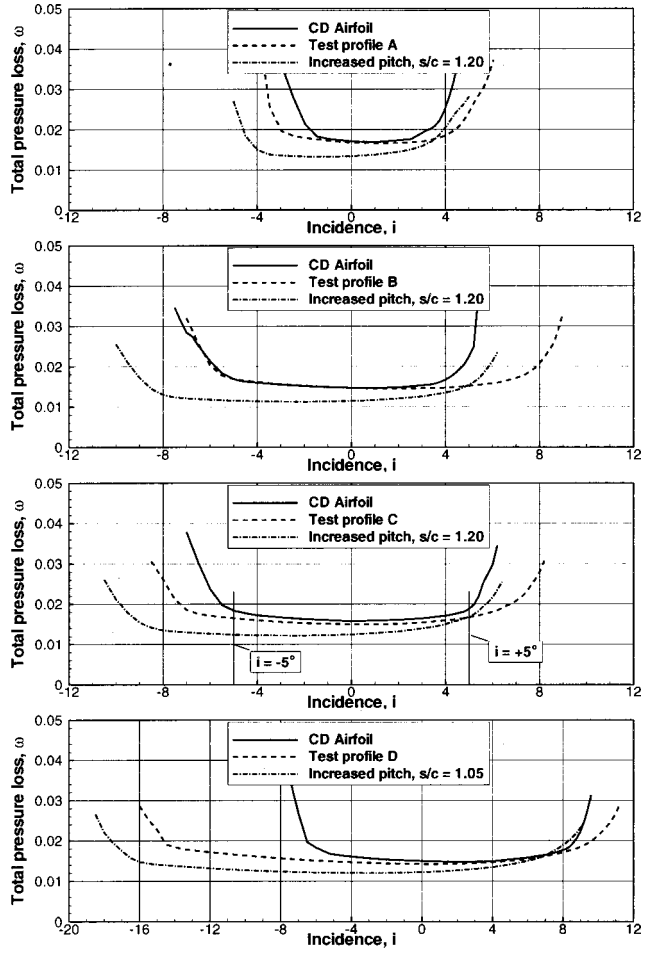

Fig. 13 Total pressure losses of CDA and new airfoils

profile C. While the CDA's peak Mach numbers are in the supersonic range, the new airfoil avoids these peaks at -5 deg and $+5$ deg incidence and stays at a moderate Mach number level. This peak reduction leads to a significant boundary layer unloading in the vicinity of the leading edge and finally results in an improvement of the separation behavior. In both diagrams in Fig. 14 downstream of $x/c=50$ percent on the suction side and downstream of $x/c=10$ percent on the pressure side, differences in the Mach number distributions can hardly be seen, so the cause for the increase in operating range has to be related to the change in the front part.

Summarizing, one can find that, compared to the reference airfoils, the new airfoil family is characterized by an increased leading edge thickness and a flattened midpart, a front-loaded Mach

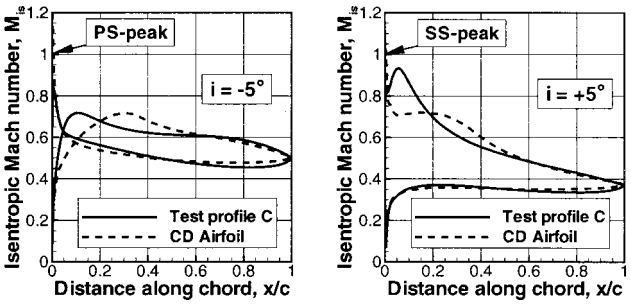

Fig. 14 Off-design Mach number distribution of CDA and new airfoils

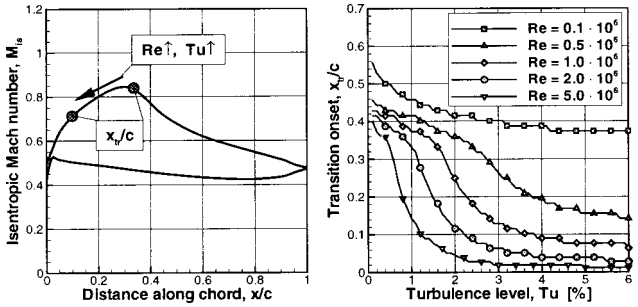

Fig. 15 Influence of Re and *Tu* on transition onset

number distribution, lower total pressure losses and considerably higher operating ranges including increased stall margin.

Influence of Reynolds Number. Compared to CDA, the new airfoil family is characterized by a front-loaded Mach number distribution. In order to emphasize that the upstream propagation of the boundary layer transition is caused by high Reynolds numbers, a corresponding numerical parameter study is presented in this chapter.

Due to the high mass flow and the resulting large dimensions in a heavy-duty gas turbine compressor, the rotor and stator chord lengths have to be considerably increased compared to aeroengine dimensions. Together with the higher inlet density at design point conditions, the profile Reynolds numbers are significantly higher ($\mathrm{Re}=2$–4×10^6). Together with the high turbulence levels in the mid and rear part of a multistage compressor, this leads to an early bypass transition of the blade boundary layer even at favorable pressure gradients [22].

In this context a numerical parameter study based on MISES calculations is presented in the right diagram in Fig. 15. Boundary layer transition is calculated for the suction side Mach number distribution shown on the left side of this figure ($M_1=0.6$). Both increasing Reynolds number and rising turbulence level result in an upstream propagation of the transition location. For low Reynolds numbers and small turbulence levels, the transition is insight a laminar separation bubble. For high Reynolds numbers and high turbulence levels the transition occurs in the bypass mode. The corresponding Mach number distribution is accelerated until $x/c=30$ percent. So, with turbulence levels $Tu\geqslant3$ percent and Reynolds numbers $\mathrm{Re}\geqslant2\times10^6$ the onset of transition migrates upstream into the region with an accelerated boundary layer to a relative chord of $x/c=7$ percent. A further increase of the turbulence level does hardly affect this transition location. It is assumed that even unsteady effects like wake passing, described for example in the work of Halstead et al. [23], do not significantly influence this early transition location, because the Reynolds number is high.

An optimal airfoil design has to take into account the change in transition location and mode. Hence, compressor airfoils, which were initially designed for aeroengine flow conditions and then transferred to heavy-duty gas turbines, do not account for these effects and do not represent the optimal solution for the heavy-duty gas turbine compressor design.

To answer the opposite question, whether the new airfoil family would also show superior behavior in flow conditions where the transition onset is located further downstream, the results of a final optimization are presented in Fig. 16. As a basis for this design test profile C was selected. The corresponding design parameters are noted in Table 3. This test profile is used as starting geometry for an optimization carried out at $\mathrm{Re}=0.8\times10^6$ and $Tu=1$ percent. The results and a comparison of both cascades are presented in Fig. 16. The top diagram shows the two geometries, the representative of the new airfoil family as a dotted line and the low-Reynolds-optimized profile as a solid line. In particular the

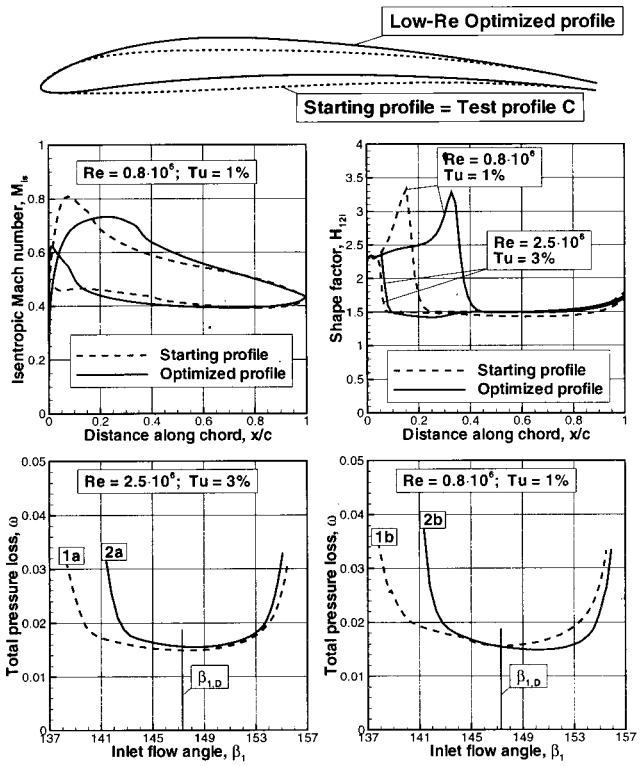

No.	profile	Re	Tu	ω_D	$\Delta\beta_1$	OBF
1a	start.	$2.5 \cdot 10^6$	3%	1.49%	16.9^o	4.18
1b	start.	$0.8 \cdot 10^6$	1%	1.56%	17.3^o	4.99
2a	optim.	$2.5 \cdot 10^6$	3%	1.56%	13.6^o	4.55
2b	optim.	$0.8 \cdot 10^6$	1%	1.55%	14.2^o	4.29

Fig. 16 Influence of Re and *Tu* on optimized profile geometry

midprofile region is characterized by an increase in camber. For the Mach number distribution at design point conditions (midleft diagram) the front-loaded suction side curve is changed to a ''roof-top'' or CDA-similar distribution with laminar suction surface flow up to 35 percent of chord. On the pressure side a deceleration in the first 20 percent of chord is visible for the optimized profile. In the rear parts of the suction and the pressure side the Mach number remained almost unaffected by the optimization. As the shape factor distributions for the low-Re numbers (midright diagram) indicate, the optimized airfoil's transition has migrated further downstream. Lower losses on the suction side due to an extension of the laminar flow region are compensated by higher losses on the pressure side due to slightly increased deceleration in the front portion. Hence, both airfoils possess almost the same design point value: $\omega_D = 1.55$ percent$\Leftrightarrow 1.56$ percent (compare $2(b) \Leftrightarrow 1(b)$ in the attached table). The objective function value for the optimized airfoil has dropped from 4.99 to 4.29. In particular, the rise in stall margin is responsible for this improvement. So, for low-Re conditions the optimized, CDA-similar profile shows better design and off-design behavior, which confirms the use of such airfoils for these boundary conditions.

In order to demonstrate that the representative of the new airfoil family still possesses superior performance at high Reynolds numbers, the objective function values for both airfoils have been calculated at $\mathrm{Re} = 2.5 \times 10^6$ and $Tu = 3$ percent. The corresponding total pressure losses are presented in the lower left diagram in Fig. 16. The test profile C (curve $1(a)$) is characterized by lower losses and a wider operating range, which results in an objective function value of 4.18 compared to 4.55 for the low-Re-optimized airfoil (curve $2(a)$).

Hence, for application in a heavy-duty gas turbine compressor with its specific boundary conditions, the new designed airfoil family has proved superior performance for design and off-design conditions. From this final low-Re optimization result, the transfer of this airfoil family to aeroengine application cannot be advised, as the controlled-diffusion airfoils in use until now seem to possess equal or even superior design and off-design behavior.

Conclusions

An important advantage is achieved by an automated design process, in which the blade geometry generation program and the flow solver are coupled to search for an aerodynamically optimized airfoil. Thereby, this process is not restricted to the ''state of the art'' experience of a design engineer. A further extension of the range of application can easily be achieved by integrating the results of additional optimizations/profile designs into the existing new airfoil family.

The superior performance of the new airfoil family for high Reynolds numbers, which is characterized by an increase in the attainable operating range and a decrease in the total pressure losses, confirms the efficiency of both the automated tool for optimized airfoil design and the formulation of the objective function. As the heavy-duty gas turbine compressor specific high Reynolds numbers lead to an upstream propagation of the boundary layer transition, an optimal velocity distribution has to account for these effects by a suction side maximum position in the front portion of the airfoil. Utilization of the newly developed airfoil family allows a reduction in blade and vane counts in comparison to conventional airfoils. For a given compressor operating range this leads to a further significant increase in efficiency.

As for each of the optimized airfoils the design and the off-design behavior is known, a complete database including the total pressure losses and the exit flow angles for different inlet flow angles, inlet Mach numbers, and AVDR values can easily be developed. Consequently, for the new airfoil family, such an extensive database has been generated in order to replace flow turning and total pressure loss correlations used in two dimensional duct- or throughflow streamline curvature codes. So, in the future, the risks in compressor development are significantly reduced by the knowledge of the exact off-design behavior during the first steps of the design process.

Nomenclature

a = basis for number of random search points
AVDR = axial velocity density ratio
c = profile chord, m
$C_1 - C_5$ = objective function coefficients
Cr = curvature
DF = diffusion factor
H_{12i} = incompressible shape factor
i = incidence $= \beta_1 - \beta_{1,D}$, deg
M = Mach number
OBF = objective function
p = pressure, Pa
$P_1 - P_3$ = spline points on pressure side
PF = penalty function
r = radius, m
Re = Reynolds number $= (w_1 \cdot c)/\nu$
s = pitch, blade spacing
$S_1 - S_3$ = spline points on suction side
t = maximum profile thickness, m
Tu = turbulence level
w = relative velocity, m/s
x = coordinate in chordwise direction, m
y = coordinate perpendicular to chordwise direction, m
β = flow angle with respect to cascade front, deg
$\Delta\beta$ = flow turning $= \beta_1 - \beta_2$, deg
$\Delta\beta_1$ = incidence range from negative to positive stall, deg
$\Delta\beta_{St}$ = incidence range from design to positive stall, deg

δ_1 = boundary layer displacement thickness, m
δ_2 = boundary layer momentum thickness, m
λ = profile (metal) angle, deg
$\Delta\lambda$ = profile wedge angle, deg
ν = kinematic viscosity, m^2/s
σ = standard deviation
ω = total pressure loss $=(p_{t1}-p_{t2})/(p_{t1}-p_1)$

Subscripts

1 = inlet plane
2 = outlet plane
80 = inner 80 percent of incidence range
D = design value
LE = leading edge
is = isentropic entity
ref = reference value in objective function
t = total, stagnation value
tr = transition
TE = trailing edge

References

[1] Johnsen, I., and Bullock, R., 1965, ''Aerodynamical Design of Axial-Flow Compressors,'' NASA SP-36.
[2] Hobbs, D., and Weingold, H., 1984, ''Development of Controlled Diffusion Airfoils for Multistage Compressor Application,'' ASME J. Eng. Gas Turbines Power, **106**, pp. 271–278.
[3] Korn, D., 1975, ''Numerical Design of Transonic Cascades,'' ERDA Research and Development Report C00-3077-72.
[4] Schmidt, E., 1979, ''Computation of Supercritical Compressor and Turbine Cascades With a Design Method for Transonic Flows,'' ASME Paper No. 79-GT-30.
[5] Stephens, H., 1979, ''Application of Supercritical Airfoil Technology to Two-Dimensional Compressor Cascades: Comparison of Theoretical and Experimental Results,'' AIAA J., **17**, No. 6, pp. 594–600.
[6] Rechter, H., Steinert, W., and Lehmann, K., 1985, ''Comparison of Controlled Diffusion Airfoils With Conventional NACA 65 Airfoils Developed for Stator Blade Application in a Multistage Axial Compressor,'' ASME J. Eng. Gas Turbines Power, **107**, pp. 494–498.
[7] Dunker, R., Rechter, H., Starken, H., and Weyer, H. B., 1984, ''Redesign and Performance Analysis of a Transonic Axial Compressor Stator and Equivalent Plane Cascades With Subsonic Controlled Diffusion Blades,'' ASME J. Eng. Gas Turbines Power, **106**, pp. 279–287.
[8] Sanger, N. L., 1983, ''The Use of Optimization Techniques to Design Controlled Diffusion Compressor Blading,'' ASME J. Eng. Power, **105**, pp. 256–265.
[9] Sanz, J., 1988, ''Automated Design of Controlled Diffusion Blades,'' ASME J. Turbomach., **110**, pp. 540–544.
[10] Goel, S., Cofer, J., and Hardev, S., 1996, ''Turbine Airfoil Design Optimization,'' ASME Paper No. 96-GT-158.
[11] Pierret, S., Van den Braembussche, R., 1997, ''Turbomachinery Blade Design Using a Navier–Stokes Solver and Artifical Neural Network,'' Reprint from 4th National Congress of Theoretical and Applied Mechanics, May 22–23, Leuven, Belgium.
[12] Lawerenz, M., 1995, ''Aerodynamische Optimierung von Strömungsmaschinen unter Verwendung direkter numerischer Optimierungsverfahreh,'' Abschlußbericht TURBOTECH-Verbundvorhaben 1.1.2.13.
[13] Schwarz, R., and Spiegel, M., 1995, ''Direkte Optimierungsverfahren zur Lösung aerodynamischer Problemstellungen bei Turbomaschinen,'' Abschlußbericht TURBOTECH-Verbundvorhaben 1.1.2.14.
[14] Küsters, B., Schreiber, H. A., Köller, U., and Mönig, R., 1999, ''Development of Advanced Compressor Airfoils for Heavy-Duty Gas Turbines: Part II—Experimental and Theoretical Analysis,'' ASME J. Turbomach., **122**, this issue, pp. 406–415.
[15] Becker, B., Schulenberg, T., and Termuehlen, H., 1995, ''The 3A-Series Gas Turbines With HBR Combustors,'' ASME Paper No. 95-GT-458.
[16] Steinert, W., Eisenberg, B., and Starken, H., 1991, ''Design and Testing of a Controlled Diffusion Airfoil Cascade for Industrial Axial Flow Compressor Application,'' ASME J. Turbomach., **113**, pp. 583–590.
[17] Giles, M., 1985, ''Newton Solution of Steady Two-Dimensional Transonic Flow,'' GTL Report No. 186, Oct.
[18] Drela, M., 1986, ''Two-Dimensional Transonic Aerodynamic Design and Analysis Using the Euler and Boundary Layer Equations,'' GTL Report No. 187, Feb.
[19] Drela, M., 1995, ''MISES Implementation of Modified Abu-Ghannam Shaw Transition Criterion,'' MISES User's Guide, MIT.
[20] Pieper, S., and Schulte, J., 1995, ''Verlustarme Verdichterauslegung (Experiment I und II),'' FVV Forschungsbericht 581.
[21] Schulenberg, T., and Zimmermann, H., 1995, ''New Blade Design of Siemens Gas Turbines,'' POWER-GEN Europe, May 16–18, Amsterdam.
[22] Mayle, E., 1991, ''The Role of Laminar-Turbulent Transition in Gas Turbine Engines,'' ASME J. Turbomach., **113**, pp. 509–537.
[23] Halstead, D. E., Wisler, D. C., Okiishi, T. H., Walker, G. J., Hodson, H. P., and Shin, H.-W., 1997, ''Boundary Layer Development in Axial Compressors and Turbines: Part 1–4,'' ASME J. Turbomach., **119**, pp. 114–127, 426–444, 225–237, 128–139.